Eur. Phys. J. D **19**, 49–56 (2002)
DOI: 10.1140/epjd/e20020054

THE EUROPEAN PHYSICAL JOURNAL D
EDP Sciences

Blue satellite bands of KRb molecule: Intermediate long-range states

H. Skenderović, R. Beuc[a], T. Ban, and G. Pichler

Institute of physics, P.O. Box 304, 10001 Zagreb, Croatia

Received 15 October 2001

Abstract. Three distinct satellite bands at 730–736 nm and a single shoulder at 755.5 nm that we assigned to KRb heteronuclear molecule are found in absorption measurements of hot K + Rb vapor. The interpretation of these bands is discussed in terms of recent *ab initio* calculations of the relevant potential curves. Semiclassical spectral simulations were performed with *ab initio* potentials and approximate transition dipole moment functions showing a good agreement with observations. The probabilities of cold molecule photoassociative formation into the external well of the double minimum $(5)0^+$ state and decay to the ground state are discussed, and relative yields of molecular formation were estimated by using quantum mechanical calculations.

PACS. 33.80.Gj Diffuse spectra; predissociation, photodissociation – 34.20.Gj Intermolecular and atom-molecule potentials and forces – 33.80.Ps Optical cooling of molecules; trapping

1 Introduction

Within last few years one can witness a large interest in KRb molecule. Quite recently, Amiot and his coworkers experimentally studied electronic states of the KRb molecule in series of experiments [1,2]. In addition, two groups published the high quality *ab initio* calculations for variety of ground and excited states [3,4]. Among heteronuclear molecules of alkali-metal elements, the KRb molecule is of particular interest because the first excited atomic levels $K(4p_{1/2,3/2})$ are in close proximity to $Rb(5p_{1/2,3/2})$ atomic levels. Hence, there is a large coupling among the electronic states connected to the $K(4s_{1/2})+Rb(5p_{1/2,3/2})$ and $K(4p_{1/2,3/2})+Rb(5s_{1/2})$ dissociating limits. Wang and Stwalley [5] pointed out that the K + Rb system is, therefore, a very good candidate for ultracold photoassociation. They discussed photoassociation into vibrational states of attractive potentials at large distances converging to the $K(4s_{1/2})+Rb(5p_{1/2,3/2})$ limits. The first experiment with ultracold ^{39}K and ^{85}Rb mixture revealed interesting heteronuclear trap loss mechanisms, but did not reveal the existence of ultracold KRb molecules [6].

By inspection of new KRb potential curves, with spin-orbit interaction [3], we found no pure long-range molecular states like it is the case with homonuclear alkali dimers [7,8]. However, there is one potential curve with two minima of which the outer one we attribute to the intermediate long-range state, $(5)0^+$.

[a] e-mail: beuc@ifs.hr

The KRb $(5)0^+$ double-well potential from the $K(4p_{3/2})$ + $Rb(5s_{1/2})$ asymptote becomes 0_g^+ double-well potential from $K(4p_{3/2})$ + $K(4s_{1/2})$ or $Rb(5p_{3/2})$ + $Rb(5s_{1/2})$ asymptotes in homonuclear K_2 or Rb_2 diatoms, respectively. It was early recognized in the K_2 molecule that the avoided crossing between two adjacent 0_g^+ states, due to the interplay between spin-orbit and electrostatic interactions is the origin of the far blue satellite band at 748.5 nm [9]. Similar satellites in Cs vapor were observed by Kusch and Hessel [10], Pichler *et al.* [11] and recently interpreted by using *ab initio* potential curves and semiclassical simulations based on Fourier transform technique by Veža *et al.* [12] and Beuc *et al.* [13].

Ab initio potential curves for the two lowest 0_g^+ excited states in Na_2 [14], K_2 [15] and in Rb_2 and Cs_2 [16] showed that one of the 0_g^+ (Hund's case (c) coupling scheme) state emerging from $n\mathrm{P}_{3/2}$ atomic level exhibits two potential wells, the one at small internuclear distance, R, and the second one in the intermediate range of R. Theoretical significance of those double-well potentials was recognized in papers by Dulieu *et al.* [17] and their possible application for cold molecule formation was described by Almazor *et al.* [18] together with spectral simulations of the whole blue wing satellite system at thermal energies.

In Figure 1 we present KRb *ab initio* potential curves [3] that are relevant for the satellite bands that we report here. These potentials represent the $(4)0^+$ and the $(5)0^+$ states in Hund's case (c) coupling, and $(3)^1\Sigma^+$ and $(2)^3\Pi$ states in Hund's case (a). The (4) and (5) 0^+ states, connected to the $K(4p_{1/2})+Rb(5s_{1/2})$ and $K(4p_{3/2})$ + $Rb(5s_{1/2})$ atomic limits exhibit avoided crossing at intermediate range and as a consequence,

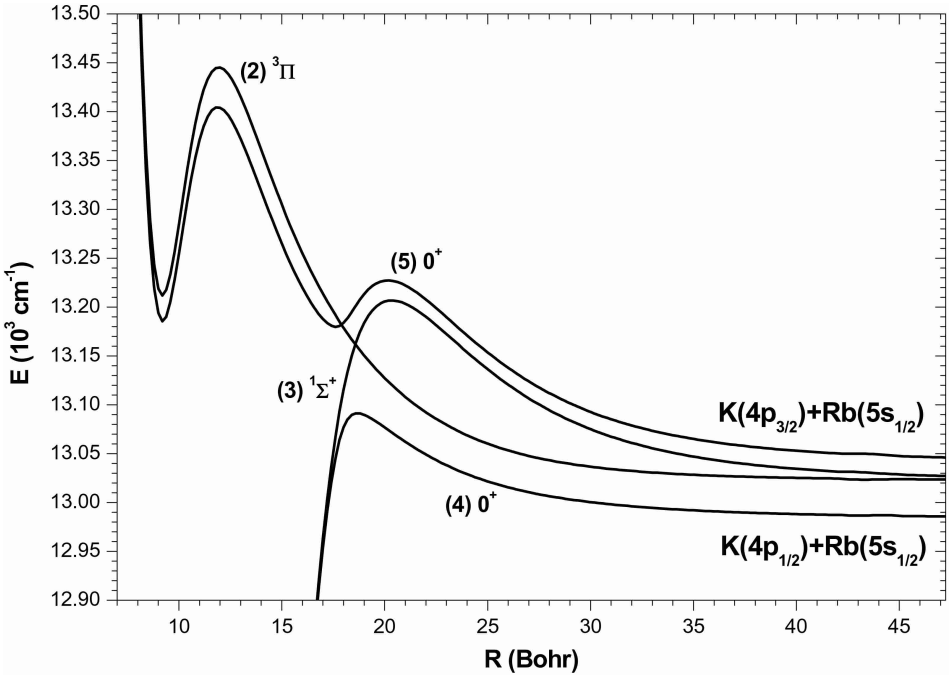

Fig. 1. KRb *ab initio* potential curves relevant for the interpretation of the observed, satellite bands, taken from reference [3].

the upper state, $(5)0^+$, shows a shallow minimum at $R \sim 17.5$ Bohr, Figure 1. This well is observed in our experiment as a satellite band and reported in present paper. An interpretation of all observed KRb satellites, observed in the very far blue wing of potassium-rubidium resonance lines, is given based on semiclassical spectral simulations. A possible dissociation of the $(5)0^+$ inner well bound levels *via* non-adiabatic mixing with $(4)0^+$ is calculated to be negligible. Hence, cold molecule formation is proposed using also these levels as intermediate stage.

The present paper is organized in 5 sections. Following introduction, the experimental details and results for absorption measurements are given in Sections 2 and 3. Semiclassical spectral simulation is presented in Section 4. In Section 5 the formation of the cold KRb molecule is theoretically investigated and the conclusion is given in Section 6.

2 Experiment

A 1:1 mixture of rubidium and potassium was used in the present study of thermal absorption. Mixed metal vapor above the heated liquid mixture consists predominantly of rubidium and potassium atoms, but there are also a small percentage of diatomic molecules, Rb_2, KRb, and K_2 (in the decreasing order of densities). The mixture was contained in a cylindrical sealed-off sapphire cell, inner diameter of 10 mm, and length of 160 mm. Due to special procedures in manufacturing the cell [19], especially in the process of sealing the sapphire windows, the cell can be used for absorption measurements up to 700 °C. The cell was located within the oven encompassed with three separated heaters, which allowed different temperatures for the central part and two identical side parts of the cell. Usually, these two side parts of the cell were kept at the same temperature, T, higher than the temperature of the central part, T_0, which was confined within about 8 mm. Therefore, the main contribution to the absorption was coming from the less dense vapor at an average temperature T. As the vapor in hotter parts was heated above the temperature of the liquid metal in the central part, thermal destruction of molecules occurred [20] in those hotter parts. This configuration of three differently heated regions inside the cell enables to obtain partly superheated vapor in two external parts of the cell.

The estimate of KRb number density can be deduced from the dissociation equilibrium equation [21]:

$$[\mathrm{KRb}] = 3.292 \times 10^{-23} \frac{g_{12}}{g_1 g_2} \sqrt{\left(\frac{m_{12}}{m_1 m_2}\right)^3} \frac{\sqrt{T}}{\sigma B_\mathrm{e}} \times \frac{\exp(1.4388 D_\mathrm{e}/T)}{\exp(-1.4388\omega_\mathrm{e}/T)} [\mathrm{K}(T_0)][\mathrm{Rb}(T_0)] \quad (1)$$

where [KRb], [K] and [Rb] are the number densities in cm^{-3}. D_e is dissociation energy, ω_e and B_e are vibrational and rotational molecular constants for the ground state of KRb, all in cm^{-1}. T is temperature in kelvin, g_1, g_2 and g_{12} are statistical weights of the K, Rb and KRb ground states, respectively. Symmetry factor, σ, is equal 1 for heteronuclear, and 2 for homonuclear molecule, m_1 is molar mass for K, m_2 for Rb and m_{12} for KRb, all in g/mol. Number densities of potassium and rubidium are taken from Nesmeyanov tables [22] and multiplied by mole fractions, ($x(\mathrm{K}) = x(\mathrm{Rb}) = 0.5$) according to Raoult's law. Molecular constants D_e, ω_e and B_e are taken from reference [23]. Similar equations apply for homonuclear dimers K_2 and Rb_2. At temperatures $T_0 = 610$ K and $T = 840$ K, for which we present our measurements,

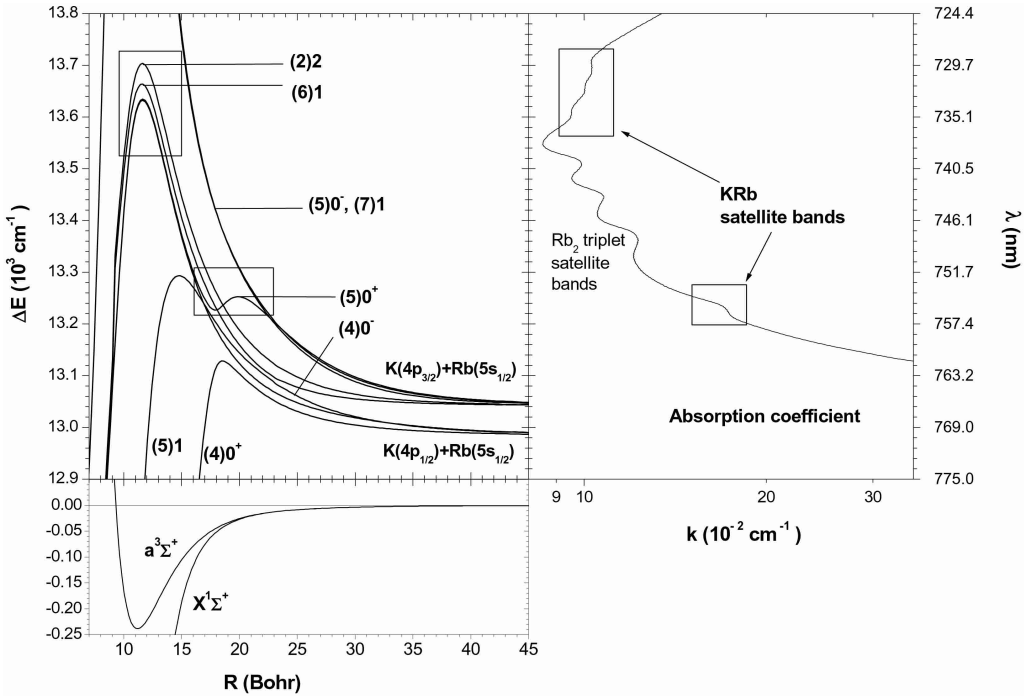

Fig. 2. Upper left panel: difference potentials of eight Hund's case (c) states connected to the $K(4p_{1/2,3/2}) + Rb(5s_{1/2})$ asymptotic limits with respect to ground triplet state, $a^3\Sigma^+$. Lower left panel: potential curves of $a^3\Sigma^+$ state and part of $X^1\Sigma^+$ state. Right panel: the absorption coefficient from the measurements at $T_0 = 610$ K and $T = 840$ K.

the KRb molecule density is estimated to be 3.2×10^{14} cm^{-3}. With molecular constants taken from literature [24,25], homonuclear dimer densities are calculated to be $[K_2] = 6.9 \times 10^{13}$ cm^{-3} and $[Rb_2] = 8.8 \times 10^{14}$ cm^{-3}. Atomic densities, $[K] = 6.5 \times 10^{15}$ cm^{-3} and $[Rb] = 2.4 \times 10^{16}$ cm^{-3}, are estimated from Nesmeyanov tables for the temperature $T_0 = 610$ K taking into account the relevant mole fractions.

In a simple absorption setup, similar to the one described earlier [26], a light from a tungsten lamp was chopped by an optical chopper, transmitted through the cell and imaged on the entrance slit of a monochromator. The monochromator (Jobin Yvon THR 1500) was equipped with a 1 200 grooves/mm grating whose scanning, by a stepper motor, was controlled by a personal computer (PC). Spectral resolution was 0.015 nm. The absolute calibration of the wavelength scale was determined using a rubidium low-pressure spectral lamp. The accuracy of the wavelength determination was better then 0.1 nm. Spectrally resolved light was detected by a photomultiplier (PMT) placed at the exit slit of the monochromator. The electrical signal from the PMT was amplified by a lock-in amplifier and fed to PC where the spectra were stored for later analysis.

3 Results

In a hot K–Rb vapor mixture spectral phenomena of both K_2 and Rb_2 dimers appear together with KRb bands. For this reason the KRb contribution to the absorption of the vapor is hard to distinguish *a priori* from the homonuclear dimers. In the investigated wavelength region (400–800 nm), KRb diffuse bands [27], (560–600 nm) and KRb satellite bands in the blue wing (725–760 nm) of potassium D2 line were observed.

We tried to enhance the KRb bands in spectra by independently varying temperatures T_0 and T. The temperatures $T_0 = 610$ K and $T = 840$ K gave enhanced and the best resolved KRb satellite bands that we could achieve. In the right panel of Figure 2 we present absorption coefficient of the vapor, derived from transmission measurements. Between these two KRb features, the Rb_2 triplet satellite bands are well pronounced [18]. The absorption towards the red rises because of the blue wing of potassium D2 line, whereas in the short wavelength region of the spectrum, the absorption background reveals the start of the Rb_2 X–B band. Because the Rb_2 X–B band decreases with increasing T, higher values of T and larger differences $T - T_0$ are more favorable for observing the KRb satellite bands. This is indeed verified by taking the spectra at various T and T_0.

On the left panel of Figure 2 relevant difference potentials in Hund's case (c) coupling for the formation of KRb satellites are shown. Curves represent the difference potentials between the excited states and lowest triplet state, $a^3\Sigma^+$, and they are labeled with the upper state designation, $(N)\Omega^{\pm}$. N is the excitation number of the state with given symmetry, Ω is the quantum number of the projection of the total electronic angular momentum onto the internuclear axis, and $\pm$ designates symmetry of $\Omega = 0$ states regarding to reflection at any plane passing through both nuclei. The potentials are taken from reference [3]. Rectangular frames are drawn to emphasize the correspondence between extrema in difference potentials and satellite bands in the spectrum. Difference potentials taking the ground singlet state, $X^1\Sigma^+$, as lower state also

Table 1. Connection between first five atomic asymptotes, Hund's case (c) electronic states and Hund's case (a) states.

K + Rb	Hund case (c)	Hund case (a)
$4\ ^2S_{1/2} + 5\ ^2S_{1/2}$	$(1)0^+$	$(1)^1\Sigma^+$
	$(1)0^-$	$(1)^3\Sigma^+$
	$(1)1$	
$4\ ^2S_{1/2} + 5\ ^2P_{1/2}$	$(2)0^+$	$(2)^1\Sigma^+$
	$(2)0^-$	$(2)^3\Sigma^+$
	$(2)1$	
$4\ ^2S_{1/2} + 5\ ^2P_{3/2}$	$(3)0^+$	$(1)^3\Pi$
	$(3)0^-$	
	$(3)1$	
	$(1)2$	
	$(4)1$	$(1)^1\Pi$
$4\ ^2P_{1/2} + 5\ ^2S_{1/2}$	$(4)0^+$	$(3)^1\Sigma^+$
	$(5)1$	$(2)^1\Pi$
$4\ ^2P_{3/2} + 5\ ^2S_{1/2}$	$(4)0^-$	$(2)^3\Pi$
	$(5)0^+$	
	$(6)1$	
	$(2)2$	
	$(7)1$	$(3)^3\Sigma^+$

give contributions to absorption but they are not shown for the reason of clarity of the figure.

On the lower panel of Figure 2, the lowest triplet state, $a^3\Sigma^+$, and a part of the singlet ground state, $X^1\Sigma$, are presented. The $a^3\Sigma^+$ state consists of two degenerate states $\{(1)0^-$ and $(1)1\}$. The correspondence between molecular state in Hund's cases (c) and (a) is shown in Table 1 for the first five dissociating limits. In the short range, both representations give virtually the same curves, except that both of $^3\Pi$ states are split into the three levels [3]. Some of the Hund's case (c) potentials exhibit avoided crossings at the distance larger than ∼15 a.u. Avoided crossing between (4) and $(5)0^+$, as already stated in the Introduction, forms the outer well in the $(5)0^+$ state, which in turn causes the satellite band at 755.5 nm, Figure 2. The other three bands, in the 730–735 nm region, originate from the extremum in $(2)^3\Pi$ state, which is comprised of four states, (see Tab. 1), split into three levels by spin-orbit interaction, Figure 2.

4 Spectral simulation

We performed the semiclassical spectral simulations taking into account transitions connecting eight excited and two ground (singlet and triplet) states, which give contribution to the absorption in the wavelength region of interest. Eight excited potentials in Hund's case (c) notation, which are included in the simulations are: $(4)0^+$, $(5)1$, $(5)0^+$, $(5)0^-$, $(4)0^-$, $(6)1$, $(7)1$ and $(2)2$ (see Fig. 2). Lower states comprise $a^3\Sigma^+\{(1)0^-, (1)1\}$ and $X^1\Sigma^+\ \{(1)0^+\}$.

For the absorption coefficient calculations of the $(1)1$, $(1)0^+ \rightarrow (5)0^+$ transitions we used the Fourier transform technique [28,29]. $(5)0^+ - (1)1$ and $(5)0^+ - (1)0^+$ difference potentials, in the energy range relevant for the 755.5 nm satellite formation have two extrema (minimum and maximum) with an inflection point in-between (see Fig. 2). They have three real Condon points, which can interfere. The observed shoulder at 755.5 nm belongs to the cusp type satellite band [12].

Table 2. The transitions included in the semiclassical simulation of the KRb absorption coefficient (Fig. 3).

	triplet transitions	singlet transitions
quasistatic approximation [30]	$(1)0^- \rightarrow (7)1$	$(1)0^+ \rightarrow (5)1$
	$(1)0^- \rightarrow (5)0^-$	$(1)0^+ \rightarrow (6)1$
		$(1)0^+ \rightarrow (7)1$
Airy approximation [30,13]	$(1)0^- \rightarrow (4)0^-$	
	$(1)0^-, (1)1 \rightarrow (6)1$	$(1)0^+ \rightarrow (4)0^+$
	$(1)1 \rightarrow (2)2$	
	$(1)1 \rightarrow (4)0^+$	
	$(1)0^-, (1)1 \rightarrow (5)1$	
Fourier transform technique [28,29]	$(1)1 \rightarrow (5)0^+$	$(1)0^+ \rightarrow (5)0^+$

The absorption coefficients for all possible transitions from one of the lower state to the $(4)0^+$, $(5)1$, $(4)0^-$, $(5)0^-$, $(6)1$, $(7)1$ or $(2)2$ upper state were calculated by using quasistatic approximation [30]. When some of these difference potentials exhibit extremum the corresponding absorption coefficient calculated in quasistatic approximation shows a first order singularity. Therefore, for the transitions connected with such potentials the Airy approximation of the linear absorption coefficient was used [13,30]. In Table 2 we summarized all transitions included in simulation.

The relevant molecular electronic transition dipole moment function $D(R)$ for each transition taken in the simulation was calculated by using semiempirical "atoms in molecules" scheme developed by Cohen and Schneider [31].

Simulation for $T = 840$ K, taking into account all possible transitions connecting $(4)0^+$, $(5)1$, $(5)0^+$, $(5)0^-$, $(4)0^-$, $(6)1$, $(7)1$, $(2)2$ excited and $a^3\Sigma^+\ \{(1)0^-, (1)1\}$, $X^1\Sigma^+\ \{(1)0^+\}$ ground states which give contribution to the absorption in the wavelength region of interest is shown in Figure 3. In the figure we present the sum of all transitions, as well as separate contributions from transitions from the ground singlet (dashed line) and triplet (solid line) states. It can be seen that singlet transitions do not contribute to the three satellite bands in 730–736 nm interval. The observed three satellite bands in this spectral region are stemming from $a^3\Sigma^+\ \{(1)0^-, (1)1\} \rightarrow (4)0^-$, $(5)0^+$, $(6)1$ $(2)2$ transitions.

Comparison between observed and calculated peak positions of triplet satellite bands are given in Table 3. Considering the fact that contributions from K + K and Rb + Rb potentials are not included in the calculation, agreement between those values is quite satisfactory. Also,

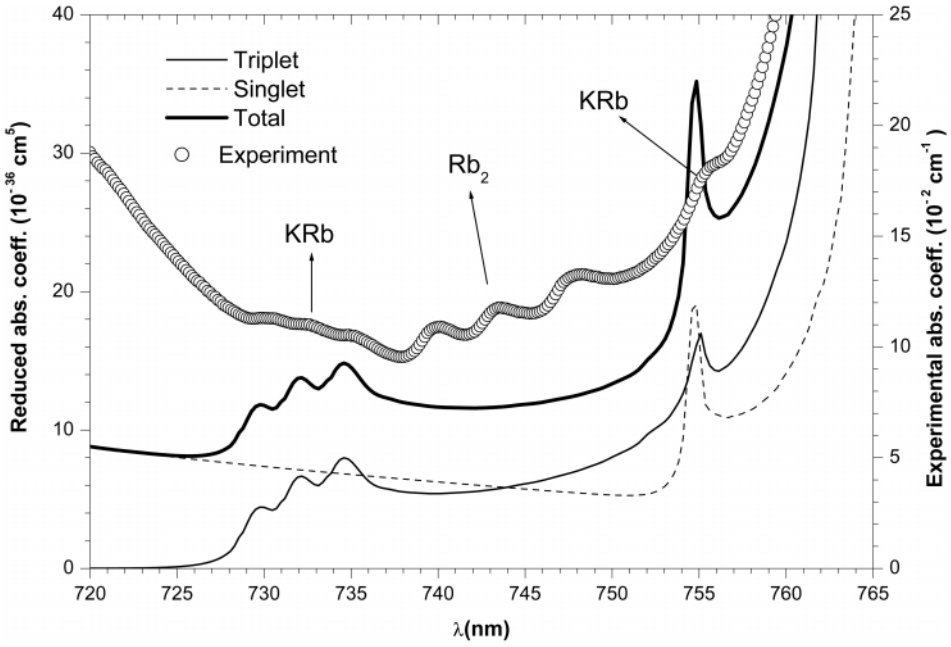

Fig. 3. Simulation of the KRb absorption coefficient in the wavelength range from 720 nm to 765 nm for $T = 840$ K, taking into account transitions connecting eight excited ($(4)0^+$, $(4)0^-$, $(5)1$, $(5)0^+$, $(5)0^-$, $(7)1$, $(6)1$, $(2)2$) and two lower ($a^3\Sigma^+$, $X^1\Sigma^+$) states. *Dashed line*: calculated absorption coefficient for the transitions from the lower singlet state. *Thin solid line*: calculated absorption coefficient for the transitions from the lower triplet states. *Thick solid line*: calculated total absorption coefficient for all transitions. *Circles*: measured absorption coefficient replotted from Figure 2.

Table 3. Observed and calculated values of satellite bands peaks.

observed	calculated values
730.07 nm	730.35 nm
732.10 nm	732.35 nm
734.74 nm	734.17 nm
755.51 nm	755.15 nm

an influence to the mismatches comes from the non-uniform temperature of vapor column.

5 Cold molecule formation

Cold molecule formation is a two-step process that associates two colliding cold atoms into bound state of the molecule. The process can be exemplified by following relations:

$$\mathrm{K} + \mathrm{Rb} + h\nu_1 \rightarrow \mathrm{KRb}^*\,(\nu', J') \tag{2}$$

$$\mathrm{KRb}^*\,(\nu', J') \rightarrow \mathrm{KRb}(\nu'', J'') + h\nu_2. \tag{3}$$

K and Rb atoms are in their ground state, $h\nu_1$ is the energy of a laser photon, blue detuned from the excited atom asymptote, and $h\nu_2$ is the energy of radiated photon. The excited electronic state $\mathrm{KRb}^*(\nu', J')$ decays radiatively to the bound levels of lowest triplet or singlet states of $\mathrm{KRb}(\nu'', J'')$, thus $\nu_2 > \nu_1$.

This scheme is depicted in Figure 4 with the $(5)0^+$ state as the excited state. Two pairs of vertical arrows indicate the two-step processes; one pair for the formation of the cold molecule in the lowest triplet state ($\nu'' = 0$), the other for the ground singlet state ($\nu'' = 84$). Our calculations show that these two vibrational levels are

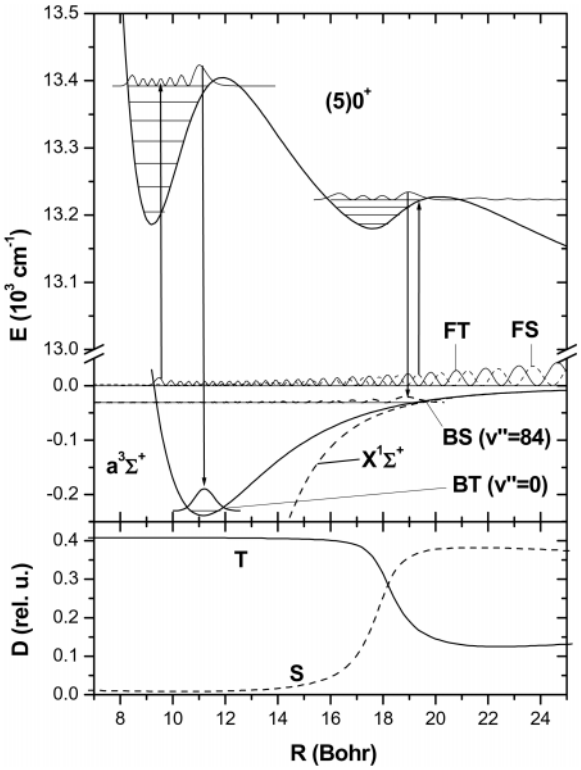

Fig. 4. Two step process of a KRb cold molecule formation, with the $(5)0^+$ state as an excited state. Two pairs of the vertical arrows indicate the formation of the cold molecule in the lowest triplet ($\nu'' = 0$) and in the lowest singlet ($\nu'' = 84$) states. FT, FS, BT and BS denotes the squared moduli, $|\Psi|^2$, of the free triplet, free singlet, bound triplet and bound singlet states, respectively. Bottom panel: the transition dipole function $D(R)$ for the transition between the $(5)0^+$ state and the lowest triplet state (solid line), and between the $(5)0^+$ state and the ground singlet state (dash line).

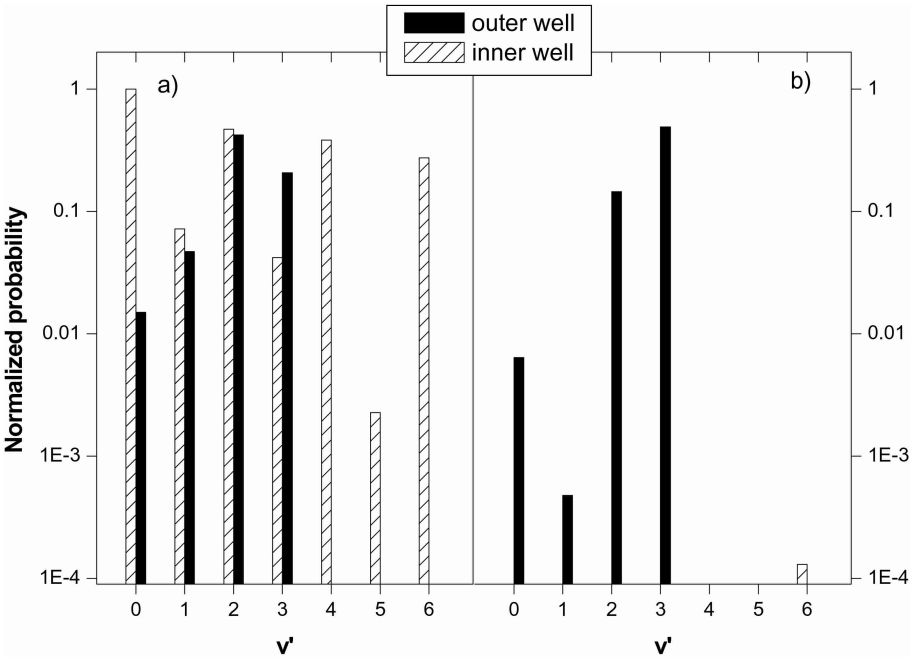

Fig. 5. The efficiency of the first step in a cold molecule formation process, equation (2). (a) FT → inner well and FT → outer well transitions, (b) FS → inner well and FS → outer well transitions.

the most populated levels. Rotationless vibrational levels calculated by uniform Fourier Grid Hamiltonian method (400 points) [32] are given both for inner and outer well of the $^{39}K^{85}Rb$ $(5)0^+$ state. The inner well binds seven and outer well four vibrational levels ($J = 0$). The wave function of $\nu' = 3$ level of the outer well, also shown in Figure 4, exhibits tunneling out towards larger R.

Details of the lowest triplet (solid line) and singlet (dashed line) state are shown in the middle section of the figure. The kinetic energy of colliding potassium and rubidium atoms is set to correspond to temperature of $T_C = 100$ μK which is typical for a standard magneto-optical trap. In approaching each other K and Rb atoms can interact either within lowest triplet or ground singlet potential. Squared moduli of free states, $|\Psi|^2$, for those two cases are labeled FT (triplet case) and FS (singlet case) in Figure 4.

In the bottom part of the Figure 4, the transition dipole moment function $D(R)$ for the transition between the $(5)0^+$ state and the lowest triplet state, and between the $(5)0^+$ state and the ground singlet state are presented by solid and dashed line, respectively. Because the $(5)0^+$ state at short distances is predominantly of triplet character (see Fig. 1), the transition dipole moment that couples inner well to the ground singlet state is essentially zero.

The efficiency of the first step in the photoassociation, equation (2), can be calculated as a square of matrix element of the transition dipole moment between lower free state and upper bound state. Four types of transition pathways are distinguishable: FT → inner well, FT → outer well, FS → inner well, and FS → outer well. We present the normalized matrix elements for the first two cases *versus* upper vibrational levels in Figure 5a and for last two cases in Figure 5b. It can be seen from the figure (note the logarithmic scale on the ordinates) that the photoassociation from FT state is possible both to the inner well and to the outer. On the contrary, photoassociation from the FS to the inner well is negligible, as already explained above. Among vibrational levels in the outer well, the most favorable photoassociation is in $\nu' = 3$ level.

The second step proceeds by radiative decay to a bound vibrational state (ν'', J''). This vibrational state can belong to the lowest electronic triplet state (labeled BT in Fig. 4) or to the ground electronic singlet state (BS in Fig. 4). Bound state vibrational energies and wave functions were calculated by the mapped Fourier grid method (300 points) [33]. Our calculations showed that the ground singlet state binds 106 rotationless vibrational levels, and the lowest triplet state binds 38 levels. Total yield of the molecule formation through photoassociation is proportional to the product of squared electronic transition dipole matrix elements for the first step and for the second step.

Cold molecules can be produced by four distinct pathways: FT → $(5)0^+$ → BT; FS → $(5)0^+$ → BT; FT → $(5)0^+$ → BS; and FS → $(5)0^+$ → BS. Among these paths, only FT → $(5)0^+$ → BT can proceed *both via* inner or outer well of the upper state. Relative yield of molecular formation as a function of final vibrational number, ν'', is given in Figure 6a for this case, with intermediate states $\nu' = 3$ of the outer well and $\nu' = 6$ of the inner well. It can be seen from the figure that the most probable photoassociation is *via* $\nu' = 6$ of the inner well to the lowest vibrational level ($\nu'' = 0$) of the $a^3\Sigma^+$ state.

The molecular formation as the function of the final ν'' for other three pathways (that can proceed only *via* outer well), are shown in Figures 6b, 6c and 6d. The intermediate state is $\nu' = 3$ of the outer well. All the graphs in Figure 6 are normalized with respect to the FT → $(5)0^+$ ($\nu' = 6$, inner) → BT($\nu'' = 0$) transition.

Since the $\nu' = 3$ level of the outer well tunnel through the tiny potential barrier, spontaneous emission alone

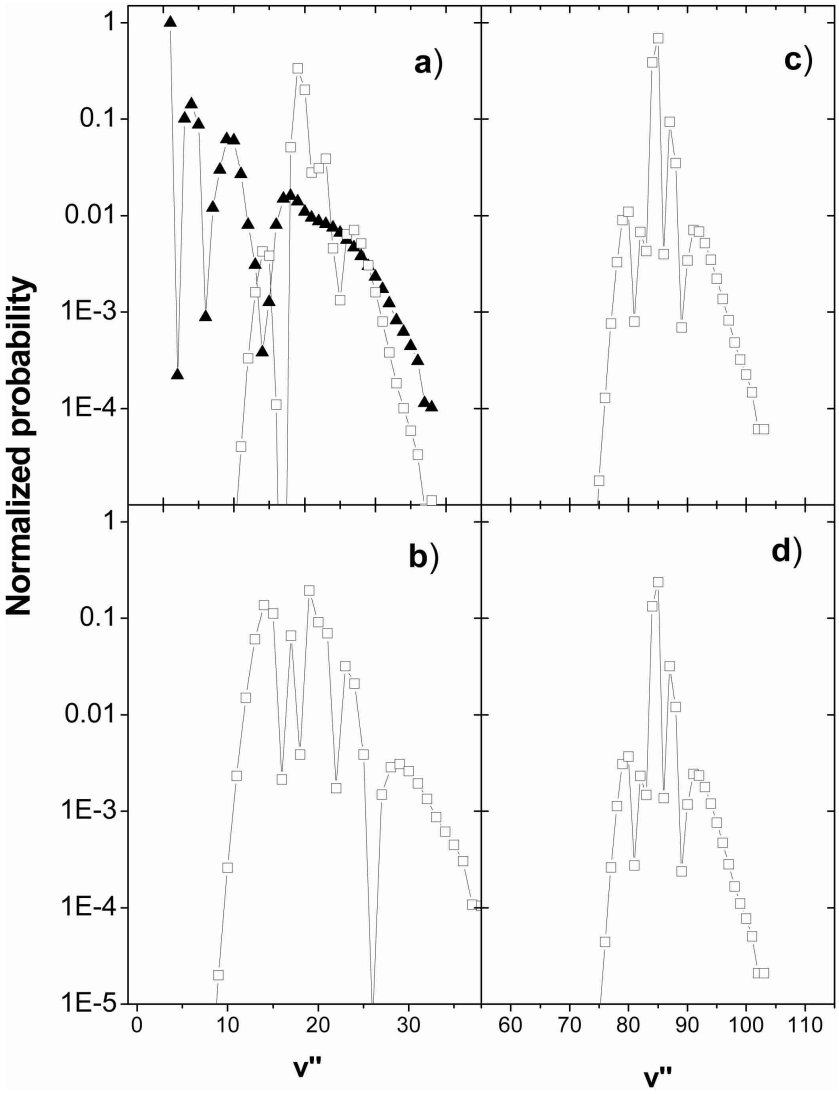

Fig. 6. Relative yield of molecular formation as a function of final vibrational number, ν'', for four distinct paths of the molecular formation. (a) FT $\rightarrow (5)0^+ \rightarrow$ BT, with intermediate states $\nu' = 3$ of the outer well (squares) and $\nu' = 6$ of the inner well (triangles), (b) FT $\rightarrow (5)0^+ \rightarrow$ BS, (c) FS $\rightarrow (5)0^+ \rightarrow$ BT and (d) FS $\rightarrow (5)0^+ \rightarrow$ BS. For last three paths the intermediate state is $\nu' = 3$ of the outer well.

would not be a good ultracold molecule formation method. However, appropriate STIRAP method [34] would most probably make the formation method more eficient.

We expect the KRb ultracold molecule formation rates to be similar as in the analogous case of Rb_2 [18]. This would mean that in order to make ultracold molecules, the densities of K and Rb atoms should be very high, of the order of $(10^{12}-10^{14})$ cm^{-3}. This requires special MOT devices and possibly some special laser techniques, which enable higher atom densities. On the other hand, KRb molecules could be formed on the surface of the cold helium clusters [35,36] and the blue satellite bands discussed in the present paper could be easily detected.

6 Conclusion

We have performed simple absorption measurements of K + Rb vapor. Satellite bands are observed in the very far blue wing of potassium D2 line but their origin is the absorption processes within KRb diatom.

Spectral simulations confirm that satellite bands in the 730–736 nm region originate from the $(1)^3\Sigma^+ \rightarrow (2)^3\Pi$ transition located at internuclear distance $R \approx 12.5$ a.u. The 755.5 nm satellite band is a result of a transition located at $R \approx 17.6$ a.u. where the upper state connected with this band, the $(5)0^+$ electronic state connected to $K(4p_{3/2}) + Rb(5s_{1/2})$ asymptote, exhibits a small well. This well was calculated to bind four vibrational levels. In the quantum calculation, we have shown that photoassociaton of cold K and Rb atom into the KRb $X^1\Sigma^+$ or $a^3\Sigma^+$ molecular electronic state is possible in a two-step process *via* outer well of the KRb $(5)0^+$ state. However, the photoassociation into the lowest vibrational level ($\nu'' = 0$) of the $a^3\Sigma^+$ state is feasible only via inner well of the upper state.

We greatly acknowledge the kind help of D. Sarkisyan and S. Ter-Avetisyan (Armenian Academy of Science, Ashtarak) for supplying the ASC and technical hints they gave us. We also thank to M. Aubert-Frécon for giving us KRb potential curves prior to publication. This work was supported by

Ministry of Science and Technology of Republic of Croatia (Program/Theme 00350101 and 00350102) and by Alexander von Humboldt-Stiftung.

References

1. C. Amiot, J. Mol. Spectrosc. **203**, 126 (2000) and references therein.
2. C. Amiot, J. Vergès, C. Effantin, J. d'Incan, Chem. Phys. Lett. **321**, 21 (2000).
3. S. Rousseau, A.R. Allouche, M. Aubert-Frécon, J. Mol. Spectrosc. **203**, 235 (2000).
4. S.J. Park, Y.J. Choi, Y.S. Lee, G.-H. Jeung, Chem. Phys. **257**, 135 (2000).
5. H. Wang, W.C. Stwalley, J. Chem. Phys. **108**, 5767 (1998).
6. L.G. Marcassa, G.D. Telles, S.R. Muniz, V.S. Bagnato, Phys. Rev. A **63**, 013413 (2000).
7. M. Movre, G. Pichler, J. Phys. B: At. Mol. Phys. **10**, 2631 (1977).
8. W.C. Stwalley, Y.H. Uang, G. Pichler, Phys. Rev. Lett. **41**, 1164 (1978).
9. R. Beuc, S. Milošević, M. Movre, G. Pichler, D. Veža, Fizika **14**, 345 (1982).
10. P. Kusch, M.M. Hessel, J. Mol. Spectrosc. **32**, 181 (1969).
11. G. Pichler, M. Movre, D. Veža, K. Niemax, in *Proc. 33rd Symp. on Molec. Spectroscopy* (Columbus, Ohio, June 12-16, 1978), TF11.
12. D. Veža, R. Beuc, S. Milošević, G. Pichler, Eur. Phys J. D **2**, 45 (1998).
13. R. Beuc, H. Skenderović, T. Ban, D. Veža, G. Pichler, W. Meyer, Eur. Phys. J. D **15**, 209 (2001).
14. S. Magnier, Ph. Millié, O. Dulieu, F. Masnou-Seeuws, J. Chem. Phys. **98**, 7113 (1993).
15. S. Magnier, Ph. Millié, Phys. Rev. A **54**, 204 (1996).
16. M. Foucrault, Ph. Millié, J.P. Daudey, J. Chem. Phys. **96**, 1257 (1992).
17. O. Dulieu, R. Kosloff, F. Masnou-Seeuws, G. Pichler, J. Chem. Phys. **107**, 10633 (1997).
18. M.-L. Almazor, O. Dulieu, F. Masnou-Seeuws, R. Beuc, G. Pichler, Eur. Phys. J. D **15**, 355 (2001).
19. D. Sarkisyan, private communication.
20. D.H. Sarkisyan, A.S. Sarkisyan, A.K. Yalanusyan, Appl. Phys. B **66**, 241 (1998).
21. P.W. Atkins, *Physical Chemistry* (Oxford University Press, Oxford, 1993).
22. A.N. Nesmeyanov, *Vapor Pressure of Elements* (Academic Press, New York, 1963).
23. C. Amiot, J. Vergès, J. Chem. Phys. **112**, 7068 (2000).
24. A.J. Ross, P. Crozet, J. d'Incan, C. Effantin, J. Phys B: At. Mol. Phys. **19**, L145 (1986).
25. C. Amiot, P. Crozet, J. Vergès, Chem. Phys. Lett. **121**, 390 (1985).
26. T. Ban, S. Ter-Avetisyan, R. Beuc, H. Skenderović, G. Pichler, Chem. Phys. Lett. **313**, 110 (1999).
27. R. Beuc, S. Milošević, G. Pichler, J. Phys. B: At. Mol. Phys **17**, 739 (1984).
28. D. Modrić, Master thesis, University of Zagreb, 2001.
29. T. Ban, H. Skenderović, R. Beuc, G. Pichler, Europhys. Lett. **48**, 378 (1999).
30. R. Beuc, V. Horvatić, J. Phys. B: At. Mol. Opt. Phys. **25**, 1497 (1992).
31. J.S. Cohen, B. Schneider, J. Chem. Phys. **61**, 3240 (1974).
32. R. Meyer, J. Chem. Phys. **52**, 2053 (1970).
33. V. Kokoouline, O. Dulieu, R. Kosloff, F. Masnou-Seeuws, Phys. Rev. A **62**, 032716 (2000).
34. K. Bergmann, H. Theuer, B.W. Shore, Rev. Mod. Phys. **70**, 1003 (1998).
35. J. Higgins, C. Callegari, J. Reho, F. Stienkemeier, W.E. Ernst, M. Gutowski, G. Scoles, J. Phys. Chem. A **102**, 4952 (1998).
36. F.R. Brühl, R.A. Miron, W.E. Ernst, J. Chem. Phys. **115**, 10275 (2001).